AIP Journal of Applied Physics

Modelling of infrared optical constants for polycrystalline low pressure chemical vapour deposition ZnO:B films

P. Prunici, F. U. Hamelmann, W. Beyer, H. Kurz, and H. Stiebig

Citation: Journal of Applied Physics **113**, 123104 (2013); doi: 10.1063/1.4795809
View online: http://dx.doi.org/10.1063/1.4795809
View Table of Contents: http://scitation.aip.org/content/aip/journal/jap/113/12?ver=pdfcov
Published by the AIP Publishing

Modelling of infrared optical constants for polycrystalline low pressure chemical vapour deposition ZnO:B films

P. Prunici,[1] F. U. Hamelmann,[1] W. Beyer,[1,2] H. Kurz,[1] and H. Stiebig[1]
[1]*Malibu GmbH & Co KG, Böttcherstrasse 7, D-33609 Bielefeld, Germany*
[2]*IEK5-Photovoltaik, Forschungszentrum Jülich GmbH, D-52425 Jülich, Germany*

(Received 5 October 2012; accepted 5 March 2013; published online 26 March 2013)

Doped zinc oxide films are of high interest in thin film solar cell technology for application as transparent conducting oxide. Rapid and detailed characterisation of ZnO thin film properties is required for quality control and optimisation of the deposited films. In the present work, a new model of dielectric functions based on the effective medium approximation (EMA) is developed and is applied for characterisation of polycrystalline boron doped zinc oxide (ZnO:B) films, deposited by low pressure chemical vapour deposition (LPCVD) technique onto glass substrates. The model takes into account that polycrystalline ZnO is considered to consist of crystal grains surrounded by depletion layers. Using this model and Fourier Transform Infrared Spectroscopy (FTIR) performed in reflection configuration over a wide mid-infrared spectral region (from 2 μm up to 25 μm), the properties of depletion layer and the bulk of the grains in ZnO can be rapidly characterised in detail, and the volume fraction of the depletion layer can be extracted. The results are in good agreement with previously presented theories of electron transport in polycrystalline materials. Using electrical measurements like conductivity and Hall techniques in addition to the optically determined parameters, predominant electron scattering mechanisms in polycrystalline films for different doping levels are identified. The measurements show the impact of the doping level on depletion layer of the crystallites. It is shown, furthermore, that under a water vapour rich environment the volume fraction of the depletion layer may increase up to 5 times and more, while the mobility of the charge carriers in the depletion layer drops drastically from about 31 $cm^2V^{-1}s^{-1}$ to about 8 $cm^2V^{-1}s^{-1}$. This indicates that water vapour exposure causes an increase of the potential barrier in the grain boundary depletion layer, limiting the electron transport across the grain boundaries to a classical thermionic emission mechanism. © *2013 American Institute of Physics*. [http://dx.doi.org/10.1063/1.4795809]

I. INTRODUCTION

Zinc oxide (ZnO) is a versatile wide band gap (about 3.37 eV at room temperature) semiconductor. It can be prepared both as a single crystal as well as, e.g., by sputtering and by low pressure chemical vapour deposition (LPCVD), as polycrystalline thin film. With appropriate dopants like gallium, aluminium, boron, or other, it is transparent in the visible spectral region and at the same time strongly (predominantly n-type) electrical conductive. As a consequence, thin ZnO films are of great interest for their use as transparent conductive oxides (TCO) in photovoltaic solar cells, flat panel displays, and other electronic devices.[1–3] Various techniques have been applied to characterise both single crystals and thin films. In the present article, we focus (besides applying Hall effect/conductivity measurements) on the characterisation using Fourier Transform Infrared Spectroscopy (FTIR). This latter technique has been used to characterise the lattice vibrations and to determine the microscopic structure of ZnO in the presence of different dopants or impurities.[4–8] Lattice and local mode vibrations are due to the interaction of the electric field of light with atomic electrical dipoles. However, the electric field of light can also interact with free charge carriers. In fact, absorption and reflection related to the free charge carriers in a doped ZnO material is usually much bigger than the dipole-related effects. In the present article, we focus on free carrier effects.

In contrast to metals where the light absorption and the reflectance edge due to free charge carriers is in ultraviolet (UV)–visible (Vis) spectral range, for doped ZnO films, this range lies in the infrared (IR) part of the spectrum. The simplest model describing the dependence of dielectric constants of a material on light frequency due to free charge carriers is the classical Drude model. This model has been successfully applied to various transparent conductive oxides (TCO)[9,10] and also to ZnO films.[11–14] The Drude model was also successfully applied in the THz time domain spectroscopy for ZnO film characterisation.[15,16] Improved models, for example employing frequency and wave vector dependent dielectric functions and taking the ionised impurity scattering into account, have also been used to describe the influence of charge carriers on optical properties.[17–19] In contrast to classical Drude model, these improved models fit better the experimental results, but they are more complicated and more constants have to be known, calculated or fitted in order to extract the density of free charge carriers and their mobility. In fact, in most of these models, it is assumed that a single-crystal material is under investigation. Nevertheless, under certain assumptions, conditions and with some restrictions they reveal appropriate and reasonable results also for

polycrystalline or nanocrystalline films[13,20,21] which are the focus of the present work.

For thin film solar cell applications, ZnO films with both high transparency and high electrical conductivity are required. Additionally, a high long term electrical and optical stability of the films is of great importance. A comprehensive review on resistivity of polycrystalline ZnO films has been presented by K. Ellmer[22] and for LPCVD ZnO films the influence of the grain size on the light scattering and electrical properties was investigated.[23] An increase of charge carrier density can be achieved by increasing the doping level of the ZnO films. On the other hand, this leads to a shift of the plasma frequency (reflection edge) towards the visible range of the spectrum making the higher doped films less optically transparent for visible light. Accordingly, an increase in charge carrier mobility can positively affect both the electrical and optical properties because a high conductivity can be reached at decreased carrier concentration and reduced optical absorption in the visible range. Improving the carrier mobility in polycrystalline films, however, may be limited by the scattering of free charge carriers by grain boundaries. For explanation of this scattering process, one assumes that on the grain surface a layer (grain boundary) exists due to a disturbed lattice with a high concentration of electronic defects located within the band gap. The charge balance usually causes depletion zones. Seto[24] described for the first time the carrier transport in polycrystalline silicon involving grain boundary effects. Later an improved model has been presented by Baccarani *et al.*[25] These theories suggest that the charge carrier mobility in polycrystalline films may strongly depend on the height of energetic barriers surrounding the grains due to the trap character of defects on the grain surface. Thus, an optimization of ZnO films for solar cell application may require a minimization of grain boundary related depletion layers. For (at least qualitative) characterisation of such depletion layers, it was recently found that the combination of FTIR and Hall measurements can be used.[20,21] We note, however, that for inhomogenous materials, like polycrystalline films, optical measurement techniques may give deviating values for free charge carrier concentration and mobility as compared to homogeneous material and that the fitting of reflectivity spectra with optical models developed for single-crystal and homogeneous materials may become questionable.

Reflection spectra over a wide spectral region performed on polycrystalline LPCVD ZnO films were published previously.[26] However, no qualitative interpretation and no detailed discussions of the recorded spectra were presented. In the present paper, it will be shown that a higher amount of information about polycrystalline LPCVD ZnO films can be extracted from FTIR measurements made in reflection configuration. One of the goals of this article is to show that the proposed dispersion model for dielectric constants in LPCVD ZnO films allows the characterisation of the depletion layer and bulk of the crystallites. This dispersion model for dielectric constants of the polycrystalline ZnO films is based on the Effective Media Approximation (EMA) theory. In contrast to previous mentioned models which are based on homogeneous materials, in the present model, the impact of the depletion layer surrounding the grains can be extracted and is measurable even if the volume fraction of the depletion layer is very small. It will be shown that the results are in a good agreement with previous theories of electron transport in polycrystalline materials.[24] We apply this dispersion model of the dielectric constants also to investigate the influence of the environment atmosphere on the crystallites morphology. On this basis, we show that this method can be used not only to characterise the crystallite properties and their morphology but also the stability of the investigated polycrystalline films under various environmental conditions.

II. EXPERIMENTAL

A Thermo Scientific Nicolet 8700 FTIR spectrometer with Vectra-Piezo interferometer has been used for the measurements. The spectrometer was purged with dry nitrogen gas before and during the measurements. A globar as a light source, a KBr beam splitter and a deuterated triglycine sulfate (DTGS) detector were used. The employed reflection unit (VeeMax from ThermoFischer) allows the measurement of the specular reflection at different angles of incidence between 30° and 80°. Reflection simulations showed that the contrast in reflection spectra is larger for smaller angles of incidence. Therefore the measurements reported here were done mostly at 30° for higher accuracy of the fits to the optical model. The measurements were averaged over 32 scans for a better signal-noise ratio. The resolution of the spectra was $4\,cm^{-1}$.

The Hall measurements were done with a RH 2010 Hall measurement system from Phystech. This setup is equipped with a C-framed electromagnet operating with a maximum field of 1.7 T where the sample with a size of maximum 3×3 cm is fixed between the poles. The specific resistivity and the Hall coefficient R_H are evaluated from measured four point resistivities at different contact configurations and magnetic field intensities. The calculation of the layer resistivity was done according to the van der Pauw method.

The samples were deposited by LPCVD technique. The ZnO films were grown on a SGG Planilux® float glass substrate from "Saint Gobain" company at a substrate temperature of about 175 °C. The precursors were diethylzinc (DEZ), hydrogen, and water vapour inserted at constant flows. The doping gas diborane (B_2H_6) was introduced into the process chamber as a 2% diborane-hydrogen gas mixture. Gas phase ratio of B_2H_6-hydrogen mixture to DEZ ([B_2H_6 mixture]/[DEZ]) was varied between 0 (low doped) and 0.4 (high doped) for different doping levels. Note that films termed "low doped" are hydrogen doped only. For more details about the applied LPCVD ZnO:B deposition parameters, see Ref. 27.

III. THEORETICAL BACKGROUND

A. Calculation of reflection spectra

Although the simulated spectra between 0° and 30° are quite similar, the actual angle of incidence was used for fitting of the calculated reflection spectra to the measured ones.

The reflectance and transmittance coefficients for *s*- and *p*-polarised light $r_{s,}$ r_p and $t_{s,}$ t_p, respectively, of a single interface between two semi-infinite media can be calculated by using the well-known Fresnel equations.[28,29] Note that all of these values are complex numbers, as well as the complex refractive indices used in Fresnel equations. In case of a film with a finite thickness, there are two interfaces and multiple reflections from the first and second interface may occur. The 2×2 matrix method is usually used to calculate the total reflectance or transmittance for such cases. For a thin film on a semi-infinite substrate, the resultant matrix M_r:

$$M_r = M_{mf} M_f M_{fs} \tag{1}$$

has to be known in order to calculate the reflectivity spectra.[28] Here, M_{mf} and M_{fs} are the interface matrices of the medium-film and film-substrate interfaces, respectively, defined as

$$M_{j,j+1} = \frac{1}{t_{j,j+1}} \begin{pmatrix} 1 & r_{j,j+1} \\ r_{j,j+1} & 1 \end{pmatrix}, \tag{2}$$

with j the medium number. M_f is the propagation matrix of the film:

$$M_f = \begin{pmatrix} \exp(ib_f) & 0 \\ 0 & \exp(-ib_f) \end{pmatrix}. \tag{3}$$

Here b_f is the phase thickness of the film f defined as

$$b_f = \frac{2\pi d_f}{\lambda} n_f \cos(\varphi_f), \tag{4}$$

where λ is the wavelength and d_f, n_f, are the thickness and complex index of refraction of the film f, and φ_f is the incidence angle of the light. Note that the wavelength and film thickness must have the same units. Knowing the resultant matrix M_r, the reflection coefficients can be readily obtained from

$$r_{p,s} = \frac{M_{r2,1}}{M_{r1,1}}. \tag{5}$$

Finally the total reflectance was calculated by

$$R = \frac{r_p \cdot r_p^* + r_s \cdot r_s^*}{2}. \tag{6}$$

Here, r_p* and r_s* denote the complex conjugates of the r_p and r_s complex numbers. It must be emphasised that r_p and r_s values are used for calculation of ellipsometrical parameters ψ and Δ which are defined as $\tan \Psi e^{i\Delta} \equiv r_p/r_s$.[29]

B. Optical model

Accordingly to Fresnel equations, the complex optical constants ($\tilde{n} = n + ik$) for all media have to be known in order to simulate the measured reflection spectra. Here n is the refractive index and k is the extinction coefficient. If the dielectric function ($\tilde{\varepsilon} = \varepsilon_1 + i\varepsilon_2$) is known, the optical constants are calculated from the relationship $\tilde{n} = \sqrt{\tilde{\varepsilon}}$. In case the optical constants are not known they have to be modelled, assumed or separately measured.

Since the measurement medium was dry nitrogen gas, optical constants for environmental medium were set as constant and equal to unity for the whole spectral range.

The optical constants of the substrate have been measured separately. Reflection spectra of the 3 millimeter thick glass substrate were measured at a small angle of incidence. Initially, the glass substrates were mechanically roughened from one side to minimise the reflections from the back side interface of the glass. By using of the Kramers-Kronig Transformation (KKT), both the index of refraction and extinction coefficient were extracted.[30]

Optical constants of the substrate are important because in case of a very thin films or very small light absorption in films, reflection from the film-substrate interface may occur and thus it should be taken into account. Correspondingly, there are some characteristic features in dielectric functions of the investigated glass substrate for frequencies lower than about 1500 cm^{-1} which cannot be neglected in reflectance calculation for transparent films.

The polycrystalline LPCVD ZnO films require an adapted model of the dielectric constants. Simple Drude model (or a modified model) is usually used to describe the optical properties of the sample when the plasma resonance wavelength is far away from lattice vibrations. The classical Drude model can be written in one of the following forms:

$$\varepsilon(\omega) = \varepsilon_\infty - \frac{\omega_P^2}{\omega^2 + i\Gamma_D\omega} = \varepsilon_\infty \left[1 - \frac{\omega_N^2}{\omega^2 + i\Gamma_D\omega}\right], \tag{7}$$

where ε_∞ and Γ_D are the high-frequency dielectric constant (we assumed $\varepsilon_\infty = 3.74$ for ZnO as a fixed parameter in all our fits) and broadening parameter, respectively. Both parameters ω_P and ω_N are known as frequency of the plasma resonance and are defined as

$$\omega_P^2 = \frac{Ne^2}{\varepsilon_0 m^*}, \quad \omega_N^2 = \frac{Ne^2}{\varepsilon_0 \varepsilon_\infty m^*} \quad \text{and} \quad \Gamma_D = \frac{e}{\mu m^*}. \tag{8}$$

From these definitions, the concentration of free charge carriers (N), and their mobility (μ) can be extracted if the constants ε_0, e, and m* (vacuum permittivity, elementary charge, and the effective electron mass, respectively) are known. Note that the relation between ω_P and ω_N is $\omega_N^2 = \omega_P^2/\varepsilon_\infty$ according to Eq. (8).

In case the plasma resonance frequency is near or lower than lattice vibrations, the polar phonons have to be taken into account in the model of the dielectric constants. The modelling of a phonon is usually made by a Lorentz oscillator:

$$\varepsilon(\omega) = \varepsilon_\infty \left[1 + \frac{\omega_{LO}^2 - \omega_{TO}^2}{\omega_{TO}^2 - \omega^2 - i\Gamma_{ph}\omega}\right], \tag{9}$$

where ω_{LO} and ω_{TO} are the frequencies of the LO and TO phonons, respectively, and the Γ_{ph} is the broadening of the oscillator. The positions and broadening of the phonons in ZnO were extensively studied previously by different

techniques like FTIR,[31,32] spectroscopic ellipsometry,[33,34] and Raman spectroscopy.[35–37] Modelling of dielectric functions for multi-phonon materials is in detail described in Ref. 38. As shown in Fig. 1, the measured reflection spectrum from a bulk, undoped ZnO single-crystal shows an acceptable agreement with theoretical simulations made with one Lorentz oscillator. Position and intensity of this oscillator agree with isotropically averaged values of the phonons in Ref. 33. Thus, we fixed the positions of the LO- and TO-phonons to $\omega_{LO} = 577\,\mathrm{cm}^{-1}$, $\omega_{TO} = 406\,\mathrm{cm}^{-1}$ for all our fits.

Finally, the dielectric function for both plasma resonance and lattice vibrations can be represented as Lorentz-Drude model:

$$\varepsilon(\omega) = \varepsilon_\infty \left[1 + \frac{\omega_{LO}^2 - \omega_{TO}^2}{\omega_{TO}^2 - \omega^2 - i\Gamma_{ph}\omega} - \frac{\omega_N^2}{\omega^2 + i\Gamma_P\omega}\right]. \quad (10)$$

Obviously, if the plasma resonance frequency has a very small value ($\omega_N \to 0$), the Lorentz model will be obtained from Eq. (10). On the other hand, in non-polar semiconductors ($\omega_{LO} = \omega_{TO}$), the Drude model will be obtained from Drude-Lorentz model.

According to the theoretical model of the electronic transport in polycrystalline semiconductors after Seto,[24] the polycrystalline ZnO films are considered as a mixture of grain nuclei with high electrical conductivity and depletion layers with lower electrical conductivity covering the grain nuclei. The dielectric constants of a mixture of different materials are usually modelled by EMA theory:

$$\frac{\varepsilon - \varepsilon_m}{\varepsilon + \gamma\varepsilon_m} = \sum_j f_j \frac{\varepsilon_j - \varepsilon_m}{\varepsilon_j + \gamma\varepsilon_m}. \quad (11)$$

Here ε denotes the dielectric constant of the mixture, ε_j and ε_m the dielectric constants of the material inclusions j in a medium m. f_j is the volume fraction part of the j-th inclusion and γ is a factor depending on inclusion geometry (for example $\gamma = 2$ for 3D spheres).[29] A requirement for EMA theory is that the inclusions have to be smaller than the wavelength of the incident light. Under certain assumptions the Eq. (11) can be rewritten in different forms. For example, in Bruggeman EMA model, the ε_m is assumed to be just ε. This model is successfully used if no individual constituent forms a clear majority of the material. Surface roughness can also be modelled by using the Bruggeman EMA theory considering a film consisting of ~50% voids and ~50% material. For simplicity, we will neglect here the roughness layer in our simulations.

Maxwell-Garnett EMA model assumes that $\varepsilon_m = \varepsilon_j$ for medium j with higher constituent. Thus, the Eq. (11) can be rewritten for Maxwell-Garnett model in the following form:

$$\varepsilon(\omega) = \varepsilon_m \frac{\varepsilon_i + 2\varepsilon_m + 2f_i(\varepsilon_i - \varepsilon_m)}{\varepsilon_i + 2\varepsilon_m - f_i(\varepsilon_i - \varepsilon_m)}. \quad (12)$$

Actually, the Maxwell-Garnett EMA is expected to be valid at low volume fractions because it is assumed that the domains are spatially separated. This latter model is usually used to characterise nanoparticles in different media. For example, Brett *et al.* used a similar model based on the Maxwell-Garnett EMA in order to characterise the Zn inclusions in nonstoichiometric ZnO film deposited by bias sputtering.[39] In case the grains are completely surrounded by the depletion layer one can assume that the grain nuclei are separated even at low or high values of the volume fractions and thus the Maxwell-Garnett model should be valid also for polycrystalline ZnO films. Thus the dielectric constants for LPCVD polycrystalline ZnO were obtained by using Eq. (12), with ε_m and ε_i calculated by Eq. (10) for both depletion layer and bulk grain respectively. We will use this dispersion model to fit the volume fraction of the depletion layer noted $f_{DL} = 1 - f_i$, the plasma resonance frequency and the broadening parameter for both grain interior and depletion layer.

IV. EXPERIMENTAL RESULTS AND DISCUSSION

Typical reflectivity spectra measured for different polycrystalline samples are presented in Fig. 2. For short wavelengths, an interference pattern is observed from which the film thickness can be extracted or estimated. In case of low

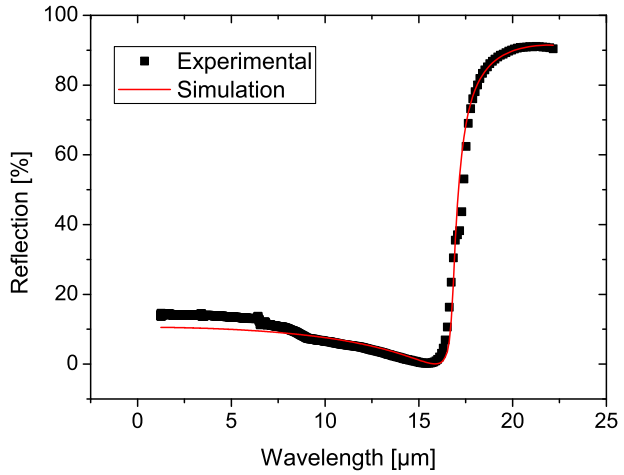

FIG. 1. Measured reflection spectrum of undoped ZnO single-crystal (squares) and simulated spectrum with one oscillator (solid line). The measured higher reflectance in spectral region below 8 μm is attributed to reflection from back side of the crystal. The fit yields a phonon broadening of 13 cm^{-1}.

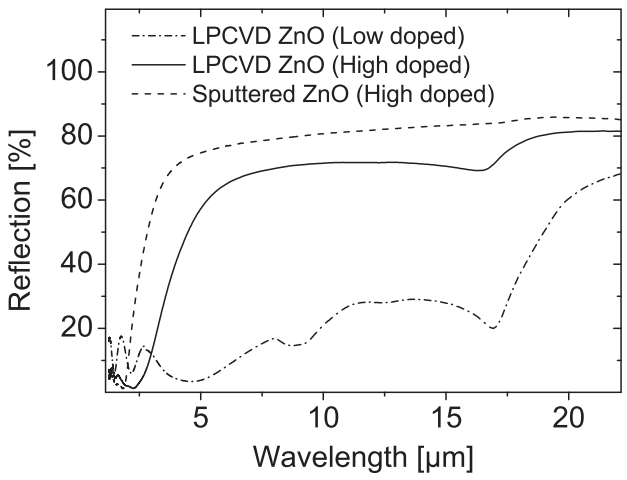

FIG. 2. Examples of measured reflection spectra for different ZnO films on glass substrates.

doped ZnO films, this pattern is observed up to the wavelength of the phonon depending on film thickness and its doping level. Next to interference pattern, the plasma reflection edge is observed. Its position and form depends on density of free charge carriers and their mobility. In addition to this edge, another reflection edge around 17 μm is seen. Actually, this position is close to the position of the LO phonons which can be measured in undoped, single-crystal ZnO, as presented in Fig. 1. Moreover, a minimum just before this edge appears. Intuitively, one can suppose that the Drude-Lorentz model could be used to model the second reflection edge and this minimum in the reflection spectrum. As presented in Fig. 3, in case of a very small value of plasma resonance frequency ($\omega_p < \omega_{TO},\omega_{LO}$), the Lorentz model can be used to simulate the reflection spectra with high reflectivity region between LO and TO phonons. This region with strong reflectance is known as *Reststrahlen* (residual rays) band reflection. Theoretical simulations with Lorentz-Drude model show that with increasing charge carrier density the plasma edge shifts to shorter wavelengths and the *Reststrahlen* band reflection will be deformed. With high values of plasma resonance, a narrower band near to TO phonon position remains, but no reflectance edge at around 17 μm as presented in Fig. 2 could be established. The simulation of the minimum in this region with Lorentz-Drude model also turns out to be very difficult. Acceptable results could not be achieved even if dispersion models are used which take the voids between grains into account or if the classical Drude model is substituted by modern improved models like Hamberg or with modified Drude models described in Refs. 17 and 18.

Assuming the dielectric constants of the polycrystalline ZnO films, with the Maxwell-Garnett EMA theory as described in Sec. III both the minima and the reflection edge in the region of the LO phonon could be reproduced. In Fig. 4, simulations of reflection spectra for different volume fraction f_{DL} of the depletion layer relative to grain bulk are presented. The higher the volume fraction is, the lower

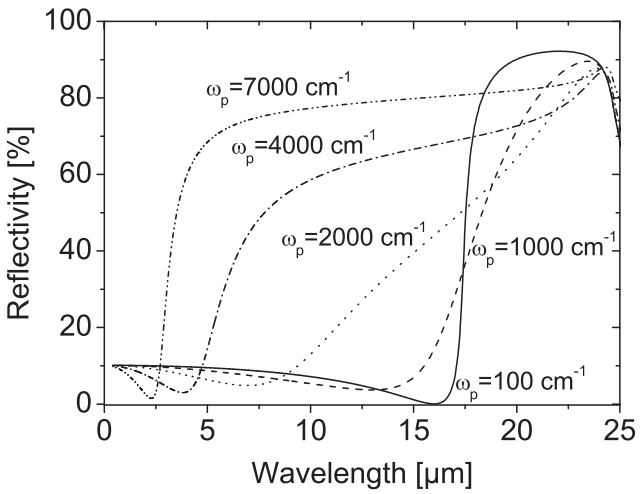

FIG. 3. Reflection spectra calculated from optical constants as modelled by Lorentz-Drude model with different plasma resonances ω_p. No minima at about 17 μm could be simulated with Loretz-Drude model and plasma resonance higher than 1000 cm^{-1}.

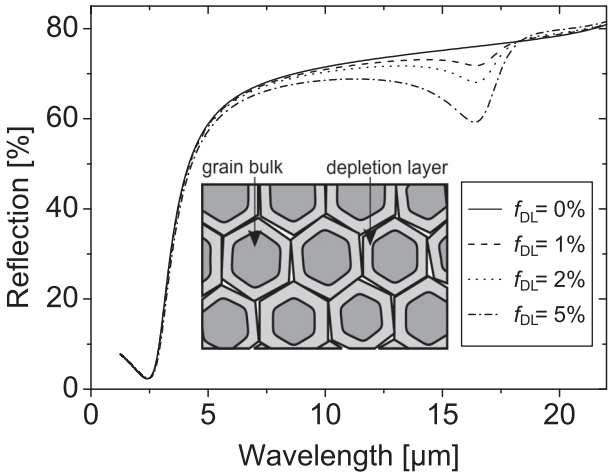

FIG. 4. Simulated reflection spectra of the polycrystalline ZnO with dielectric constants calculated by Maxwell-Garnett EMA model with different volume fraction f_{DL} values of the depletion layer. For grain bulk, a plasma resonance ($\omega_{p,1}$) of 7000 cm^{-1} and a broadening factor (Γ_1) of 900 cm^{-1} were used. For depletion layer, 1000 cm^{-1} was used for the plasma resonance frequency ($\omega_{p,2}$) and 4500 cm^{-1} for its broadening (Γ_2).

minima in reflectance spectrum at ~17 μm are observed. From reflection spectra presented in Fig. 2 it is seen that for sputtered ZnO films, the structure near 17 μm is barely visible. Possible reasons for this difference between LPCVD and sputtered films could be that in sputtered ZnO the crystallites are distorted and not as well defined as in LPCVD ZnO films, that the volume fraction of the depletion layer is very small and that the Maxwell-Garnett EMA theory is not valid for such grain dimensions and geometries. We note that the structure of LPCVD ZnO is generally quite different from that of sputtered ZnO, since in particular the mass density is lower and there is a higher concentration of interconnected voids. Presumably because the 17 μm structure in the reflectance spectrum of the sputtered films is quite small, it was not observed earlier.[13] In contrast to sputtered ZnO films, LPCVD ZnO films have a more pronounced minimum and second reflection edge revealing a higher volume fraction of the depletion layer. Therefore, it appears important to characterise the depletion layer of the grains in LPCVD ZnO films.

Examples of the optical constants modelled for grain nuclei ($f_{DL} = 0\%$) in comparison to depletion layer ($f_{DL} = 100\%$) are depicted in Fig. 5. Additionally, optical constants for films with intermediate values of volume fraction ($f_{DL} = 1$, 2, 3, and 5%) are presented as well. The phonon positions were assumed to be the same for both grain nuclei and depletion layer, while the plasma resonance frequency and its broadening are different. A plasma resonant frequency ($\omega_{p,1}$) of 7000 cm^{-1} and a broadening (Γ_1) of 900 cm^{-1} are assumed for grain nuclei (high conducting volume), while 1000 cm^{-1} and 4500 cm^{-1} are assumed for plasma resonance frequency ($\omega_{p,2}$) and its broadening (Γ_2), respectively, for the depletion layer (low conducting volume). This assignment will be used further in this article. The strong contrast (especially in *Reststrahlen* band reflection between LO and TO phonons) between optical constants for "high conducting" and "low conducting" regions induces a strong difference in

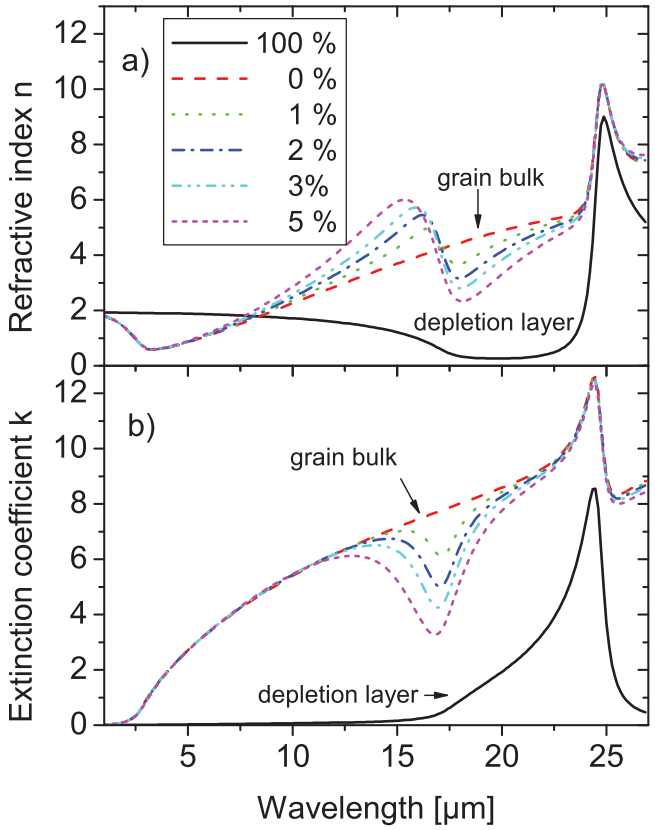

FIG. 5. The optical constants calculated by Maxwell-Garnett EMA theory using the Lorentz-Drude model for grain nuclei ($f_{DL} = 0\%$), depletion layer ($f_{DL} = 100\%$), and polycrystalline films with different volume fraction of depletion layer ($f_{DL} = 1\%$, 2%, 3%, and 5%). (a) Refractive index n and (b) extinction coefficient k as function of wavelength. The high differences in optical constants are observed especially for region between LO and TO phonons (17-23 μm). Plasma resonance frequencies and their broadening factors for grain bulk and depletion layer are the same as in Fig. 4.

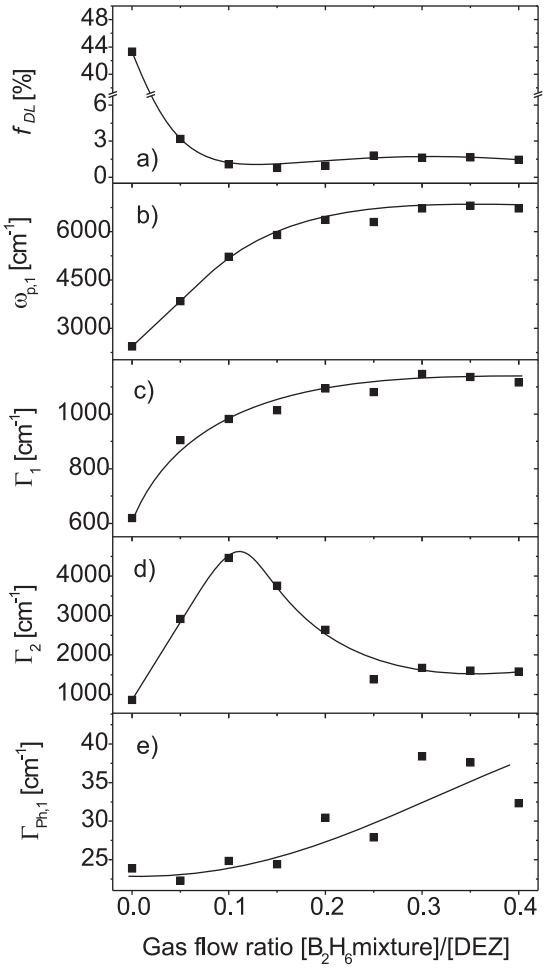

FIG. 6. Results of the fits for LPCVD ZnO:B films. (a) The volume fraction of the depletion layer f_{DL}, (b) the plasma resonance frequency $\omega_{p,1}$ in grain bulk, (c) the broadening factor Γ_1 in grain bulk, (d) the broadening factor Γ_2 for the depletion layer, and (e) the broadening factor of the phonon $\Gamma_{ph,1}$ in the grain bulk, as a function of diborane flow rate. The solid lines are a guide for the eye.

simulated optical constants and, respectively, in simulated reflection spectra for grain bulk and depletion layer. Thus, it is not surprising that even at very low volume fraction of the depletion layer a measureable change in the reflectivity spectrum can be observed, as seen in Fig. 4.

Furthermore, the simulated spectra were fitted to reflectivity spectra measured between 2 μm and 25 μm for LPCVD ZnO:B films with different doping levels. It should be mentioned that for a better definition of the depletion layer, the plasma resonance position for depletion layer was fixed to 1000 cm^{-1} (for $m^* = 0.265m_0$, $N = 3 \times 10^{18}$ cm^{-3}). The film thicknesses were also monitored with a profilometer and compared to the fitted values. For highly doped films, the thickness was fixed as measured by profilometry. The values of the film thickness become less critical in IR spectral region for films thicker than 2 μm with high doping concentrations. The reflection from the ZnO/substrate interface is very small for such films, because the largest part of the light will be reflected from the first interface (air/ZnO) and because of high light absorption in the film by free charge carriers. Fitting results of the measurements are presented in Fig. 6. The volume fraction of the depletion layer (see Fig. 6(a)) was observed to be higher for undoped samples than for doped ones. The volume fraction value correlates with depletion layer thickness if one assumes that the grain dimensions are constant for the investigated films. As observed from Scanning Electron Microscopy (SEM) pictures, the surface structures and roughness are nearly the same for all investigated films, justifying our assumption of near constant grain size. With increasing of the doping level, the volume fraction of the depletion layer decreases and then remains nearly constant. This is in a good agreement with the transport model in polycrystalline materials, since at lower charge carrier densities the electron traps at the grain boundary are only partially filled and the thickness of the depletion layer is larger. With increasing of the charge carrier density, the charge traps at the boundary will be filled, decreasing the thickness of the depletion layer. Thus for higher charge carrier densities, the depletion layer width will be narrower, enabling quantum-mechanical tunnelling of the electrons through the depletion layer.

The plasma resonance frequency for bulk grain, which correlates with charge carrier density, shifts, as expected, with increasing diborane flow towards shorter wavelengths (see Fig. 6(b)). At low doping levels, the plasma resonance frequency changes nearly linearly with rising diborane flow,

while at high doping levels a saturation effect is observed. This saturation may be due to decreasing of doping efficiency or because of a saturation effect of the boron incorporation in ZnO films.

The same tendency is found for broadening parameter of the Drude model inside the grain bulk as presented in Fig. 6(c). Since the mobility is inverse proportional to the broadening parameter, a decrease of the mobility with increasing doping level is observed. The continuous decrease of the mobility with rising diborane flow suggests that the predominant scattering mechanism inside the bulk grains is scattering by ionised impurities and on defects. An increase of the defect density can also be concluded from the phonon broadening in bulk grains (see Fig. 6(e)). The fitted values of the phonon broadening in the depletion layer were very small, except for the case of the lowest doping, where the volume fraction of the depletion layer was higher. For this sample, the phonon broadening was found at about $12\,cm^{-1}$.

The fitted value of the plasma peak broadening in the depletion layer is depicted in Fig. 6(d). We find that this dependence is very similar to the dependence of the potential barrier height on doping concentration as presented by Seto.[24] This is not surprising, because as stated by the latter author, the mobility is exponentially dependent on the barrier height while the carrier concentration is less affected, since the charge carrier density depends on the shape of the potential barrier only.[24]

In order to extract the density of free charge carriers and their mobility from the fit parameters, the value of the effective mass of the electron in ZnO is needed. However, due to the nonparabolicity of the conduction band, the effective mass of the electron (m^*) in ZnO depends on the charge carrier density. The dependence of the electron effective mass in ZnO on the doping concentration is still an issue. There is some work in the literature concerning this topic. For example, Baer calculated the electron effective mass in ZnO from free carrier Faraday rotation.[40] For low concentration of charge carriers ($10^{18}\,cm^{-3}$), the electron effective mass was found to be $0.23\text{-}0.24m_0$ and for a concentration of about $1.5\times10^{19}\,cm^{-3}$, $0.25m_0$ was found. For concentrations higher than $10^{20}\,cm^{-3}$, m* is believed to be higher, around $0.28m_0$, $0.32m_0$, or even $0.5m_0$ for very high electron densities.[13,20,41] If one considers the electron effective mass equal to $0.265m_0$ as a mean value between $0.25m_0$ and $0.28m_0$, the extracted electrical properties from the Drude model should be reasonable at least in the concentration region from 10^{19} to $10^{20}\,cm^{-3}$. The results for the bulk of the grains are presented in Fig. 7 together with results of Hall measurements for a comparison. For low doping levels, a strong difference between Hall mobility and optical mobility is observed. Again this agrees with electron transport theory in polycrystalline materials. A large volume fraction of depletion layer increases the magnitude of the scattering at grain boundaries and this scattering mechanism apparently becomes predominant.

The magnitude of the scattering at grain boundaries does not depend on doping level only but also on grain size and on the number of electron traps on the grain boundary. With changing environment atmosphere, the concentration

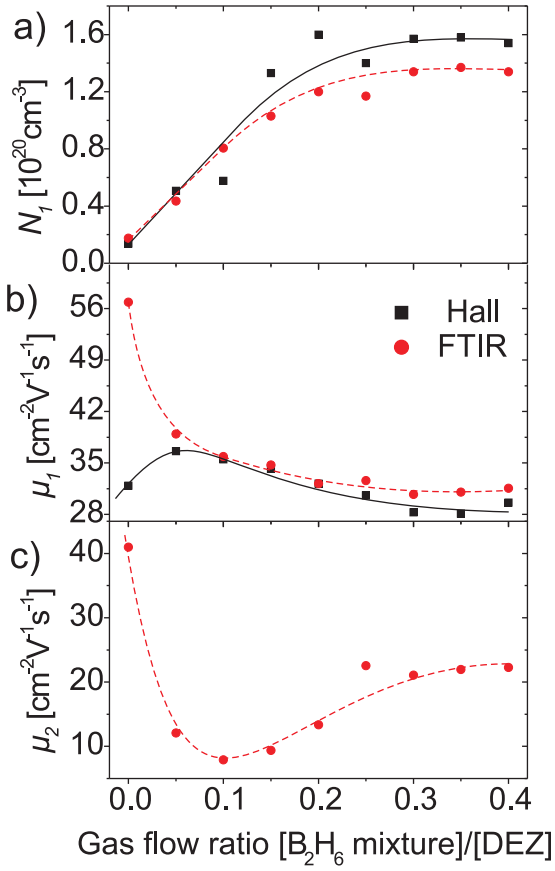

FIG. 7. Comparison between Hall and optically measured results for the LPCVD ZnO:B films deposited on glass substrates. (a) Density of charge carriers N_1 in the grain bulk, (b) the mobility of charge carriers inside the grain bulk, and (c) the mobility of the charge carriers in the depletion layer as a function of diborane flow. The solid and dashed lines are a guide for the eye.

of electron traps at the grain boundaries may change and thus a broadening or a narrowing of the depletion layer may occur.[42] Consequently, the potential barrier on the grain surface may change. We note that many types of gas sensors are working on this principle.[43]

As an additional demonstration that the FTIR technique is able to characterise the depletion layer of the grains we measured IR reflectivity spectra of polycrystalline LPCVD ZnO films by FTIR before and after exposure of the samples to an environmental atmosphere with 85% humidity at 85 °C for 24 hours. This is the so called "Damp-Heat" – test, usually used in thin film solar cell industry as a test of long term stability. Beyer *et al.* showed by effusion measurements that gas diffusion in LPCVD, ZnO films is much higher than in single-crystal or in sputtered films.[27] Using this fact, one can assume that molecules of water and oxygen adsorbed between grains may change the concentration of electron traps at the grain surface, changing the morphology of the depletion layer. Typical results of the measured and simulated spectra are presented in Fig. 8. Full and detailed results of these measurements will be presented later in a future article, but an example of the impact of this test on the film property will be presented here.

Since the measurements were all performed on the same sample one can assume that the film thickness remains the same before and after "Damp-Heat" test, and therefore, it

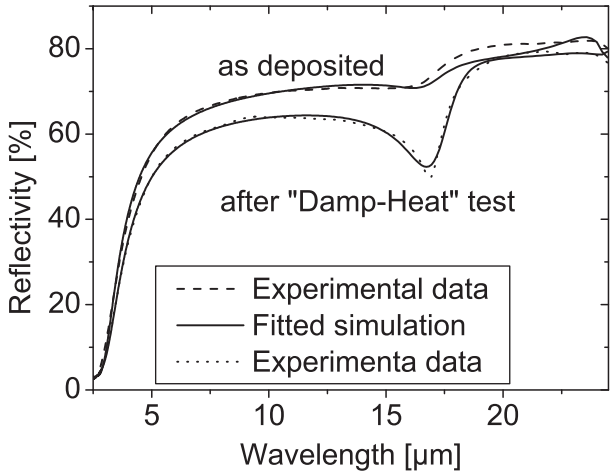

FIG. 8. The change in reflection spectra for LPCVD ZnO:B film measured before and after "Damp-Heat" experiment. The minimum measured at about 17 μm gets considerably deeper after "Damp-Heat" experiment indicating large changes in depletion layers.

was fixed as a constant, as measured by profilometry. The average grain dimension in the film is also assumed to remain constant. All other parameters were fitted to the measured reflection spectra. The results of optical and Hall measurement are presented in Table I for comparison. The strong modification of the depletion layer by the humid air during the test is evident. The volume fraction of the depletion layer drastically changes from 1.5% up to more than 6%. Thus, the thickness of the depletion layer is increased. It should be noted that for such samples, the Maxwell-Garnett EMA is much more suitable since with broadening of the depletion layer the probability that the grain nuclei are isolated increases. Additionally, the grain nuclei become smaller meeting better the requirement of the Maxwell-Garnett EMA theory, namely that the grain nuclei have to be smaller than the wavelength of the incident light. This can be observed also experimentally in calculated Mean Square Errors (MSE) values, indicating a much better fitting quality for measurement of the treated sample (see Table I). The electrical parameters of bulk grain did not change as much as measured by FTIR spectroscopy. Just a slight decrease of carrier density and of their mobility could be observed. In depletion layers, the density of charge carrier slightly increases while their mobility is strongly decreased. For the "as deposited" sample, the Hall results agree rather with electrical properties extracted from dielectric functions modelled for the bulk grains. The measured sheet resistances by optical (for grain bulk values) and electrical methods are very close at 9.7 Ω and 8.9 Ω, respectively, indicating a weak influence of the depletion layer on electron transport across the grain boundaries. This may indicate that both thermionic emission across the grain barriers and quantum-mechanical tunnelling through the barriers by electrons may occur, which is common for high doped films. The electrical properties of the bulk of the grains change just slightly after "Damp-Heat" test in contrast to electrically measured sheet resistance which increases from 8.9 Ω up to 41.6 Ω. At the same time, the Hall mobility of the carrier drops, becoming comparable with electron mobility values obtained for depletion layer, as measured by FTIR. The mechanism of quantum-mechanical tunnelling of the electrons becomes less pronounced because of the increase in potential barrier and of the width of the depletion layer. Thus thermionic emission across the grain barriers becomes likely predominant after "Damp-Heat" treatment. It is obvious that in such case the scattering at the grain boundaries is the most dominant scattering mechanism limiting the electrical conductivity of the film on the macroscopic scale also for high doping concentrations.

V. CONCLUSIONS

Reflectivity measurements in MID-IR region have been performed on LPCVD ZnO:B thin films on glass substrates. This is an easy to perform, rapid, non-destructive, and non contact measurement method. The proposed dispersion model based on Maxwell-Garnett EMA theory was successfully used to model the dielectric constants of the polycrystalline LPCVD ZnO films consisting of crystallites covered by depletion layers. The fits of the simulated data to experimental results provided important information like charge carriers density and charge carrier mobility in both bulk and in the depletion layer of the grains. Moreover, the volume

TABLE I. Experimental results before and after "Damp-Heat" experiment. In the first column of the FTIR results, the direct fitting parameters f_{DL}, $\omega_{p,1}$, Γ_1, $\Gamma_{Ph,1}$, $\omega_{p,2}$, Γ_2, $\Gamma_{Ph,2}$ are given. In second column of the FTIR results, the extracted electrical values (using an effective electron mass of 0.28 m_0) from the fitting parameters are presented for comparison with conductivity/Hall results.

	As deposited			After "Damp-Heat" experiment		
	FTIR		Hall	FTIR		Hall
R_{Sq} [Ω]		9.7[a]	8.9		11.58[a]	41.6
Volume fraction f_{DL} [%]	1.5			6.42		
$\omega_{p,1}$ [cm^{-1}], n [10^{20} cm^{-3}]	6204.84	1.2 (n)	1.36 (n)	6180.71	1.19 (n)	0.972 (n)
Γ_1 [cm^{-1}], μ [$cm^2V^{-1}s^{-1}$]	1076.49	31 (μ)	30.4 (μ)	1246.09	26.77 (μ)	9.11 (μ)
$\Gamma_{Ph,1}$ [cm^{-1}]	28.2			56.04		
$\omega_{p,2}$ [cm^{-1}], n [10^{20} cm^{-3}]	1003.12	0.031 (n)		1316.58	0.054 (n)	
Γ_2 [cm^{-1}], μ [$cm^2V^{-1}s^{-1}$]	1092	30.54 (μ)		4425.49	7.54 (μ)	
$\Gamma_{Ph,2}$ [cm^{-1}]	0.01			0.01		
MSE	1.3714			0.3541		

[a]Values are calculated from properties of grain bulk ($\omega_{p,1}$ and Γ_1).

fraction of the depletion layer could be extracted as well. The large difference in optical constants for high and low conductive ZnO regions (bulk and depletion layer) allows the characterisation of the crystallites even at low volume fractions of the depletion layer. Despite several assumptions and fit parameters, reasonable results agreeing with previous work was obtained.

The results for samples with different doping concentrations are in a good agreement with previously presented theories for electron transport in polycrystalline semiconductors. The origins and causes of the differences between electrical and spectroscopic measurement results could be explained, demonstrating the usability of the Maxwell-Garnett model for polycrystalline ZnO films. The "Damp-Heat" tests clearly demonstrate the possibility and the importance of presented technique to characterise not only the optical and electrical properties of the bulk and depletion layer of the grains but also the long term stability and reactivity of the investigated polycrystalline films. We suppose that this dispersion model can be extended to some other polycrystalline films in order to characterise depletion layers of crystallites.

ACKNOWLEDGMENTS

Part of the work was financed by the Bundesministerium für Umwelt, Naturschutz und Reaktorsicherheit (BMU) under Contract No. 03276937 (LIMA project) and by the state of Nordrhein-Westfalen under Project No. EN/1008B (TRISO project).

[1]Z. C. Zin, I. Hamberg, and C. G. Granqvist, J. Appl. Phys. **64**, 5117 (1988).
[2]T. Kamiya and M. Kawasaki, MRS Bull. **33**, 1061 (2008).
[3]X. Jiang, F. L. Wong, M. K. Fung, and S. T. Lee, Appl. Phys. Lett. **83**, 1875 (2003).
[4]S. J. Jokela, M. D. McCluskey, and K. G. Lynn, Physica B **340–342**, 221 (2003).
[5]M. D. McCluskey, S. J. Jokela, K. K. Zhuravlev, P. J. Simpson, and K. G. Lynn, Appl. Phys. Lett. **81**, 3807 (2002).
[6]B. M. Keyes, L. M. Gedvilas, X. Li, and T. J. Coutts, J. Cryst. Growth **281**, 297 (2005).
[7]X. Li, B. Keyes, S. Asher, S. B. Zhang, S.-H. Wei, T. J. Couttts, S. Limpijumnong, and C. Van de Walle, Appl. Phys. Lett. **86**, 122107 (2005).
[8]D. Scarano, S. Bertarione, G. Spoto, A. Zecchina, and C. Otero Arean, Thin Solid Films **400**, 50 (2001).
[9]C. C. Marcel, N. Naghavi, G. Couturier, J. Salardenne, and J. M. Tarascon, J. Appl. Phys. **91**, 4291 (2002).
[10]I. Hamberg and C. G. Granqvist, J. Appl. Phys. **60**, R123 (1986).
[11]I. H. Kim, K. S. Lee, T. S. Lee, J. H. Jeong, B. Cheong, Y. J. Baik, and W. M. Kim, J. Appl. Phys. **100**, 063701 (2006).
[12]C. A. Wolden, T. M. Barnes, J. B. Baxter, and E. S. Aydil, J. Appl. Phys. **97**, 043522 (2005).
[13]S. Brehme, F. Fenske, W. Fuhs, E. Nebauer, M. Poschenrieder, B. Selle, and I. Sieber, Thin Solid Films **342**, 167 (1999).
[14]F. Ruske, A. Pflug, V. Sittinger, B. Szyszka, D. Greiner, and B. Rech, Thin Solid Films **518**, 1289 (2009).
[15]T. I. Jeon, D. Grischkowsky, A. K. Mukhejee, and R. Menon, Appl. Phys. Lett. **79**, 4142 (2001).
[16]J. Han, A. K. Azad, and W. Zhang, J. Nanoelectron. Optoelectron. **2**, 222 (2007).
[17]I. Hamberg and C. G. Granqvist, J. Appl. Phys. **59**, 2950 (1986).
[18]B. E. Sernelius, Phys. Rev. B **36**, 1080 (1987).
[19]D. Mergel and Z. Qiao, J. Phys. D: Appl. Phys. **35**, 794 (2002).
[20]J. Steinhauser, S. Fay, N. Oliveira, E. Vallat-Sauvain, D. Zimin, U. Kroll, and C. Ballif, Phys. Status Solidi A **205**, 1983 (2008).
[21]J. Steinhauser, S. Fay, N. Oliveira, E. Vallat-Sauvain, and C. Ballif, Appl. Phys. Lett. **90**, 142107 (2007).
[22]K. Ellmer, J. Phys. D: Appl. Phys. **34**, 3097 (2001).
[23]S. Fay, J. Steinhauser, N. Oliveira, E. Vallat-Sauvain, and C. Ballif, Thin Solid Films **515**, 8558 (2007).
[24]J. Y. Seto, J. Appl. Phys. **46**, 5247 (1975).
[25]C. Baccarani, B. Ricco, and G. Spadini, J. Appl. Phys. **49**, 5565 (1978).
[26]W. M. Hlaing Oo and M. D. McCluskey, Mater. Res. Soc. Symp. Proc. **864**, E4.40.1 (2005).
[27]W. Beyer, U. Breuer, F. Hamelmann, J. Hüpkes, A. Stärk, H. Stiebig, and U. Zastrow, Mater. Res. Symp. Proc. **1165**, M05–24 (2009).
[28]O. S. Heaven, *Optical Properties of Thin Solid Films* (Dover, New York, 1991).
[29]*Handbook of Ellipsometry*, edited by H. G. Tompkins and E. A. Irene (William Andrew Publishing, Norwich, NY, and Springer, Heidelberg, Germany, 2005).
[30]V. Lucarini, J. J. Saarinen, K.-E. Peiponen, and E. M. Vartiainen, *Kramers-Kronig Relations in Optical Materials* (Springer, Berlin/Heidelberg, 2005).
[31]R. J. Collins and D. A. Kleinman, J. Phys. Chem. Solids **11**, 190 (1959).
[32]E. F. Venger, A. V. Melnichuk, L. L. Melnichuk, and Y. A. Pasechnik, Phys. Status Solidi B **188**, 823 (1995).
[33]C. Bundesmann, Ph.D. thesis, Leipzig University 2005 (Shaker, Aachen, 2006).
[34]N. Ashkenov, B. N. Mbenkum, C. Bundesmann, V. Riede, M. Lorenz, D. Spemann, E. M. Kaidashev, A. Kasic, M. Schubert, M. Grundmann, G. Wagner, H. Neumann, V. Darakchieva, H. Arwin, and B. Monemar, J. Appl. Phys. **93**, 126 (2003).
[35]B. H. Bairamov, A. Heinrich, G. Irmer, V. V. Toporov, and E. Ziegler, Phys. Status Solidi B **119**, 227 (1983).
[36]T. C. Damen, S. P. S. Porto, and B. Tell, Phys. Rev. **142**, 570 (1966).
[37]F. Decremps, J. Pellicer-Porres, A. M. Saitta, J. C. Chervin, and A. Polian, Phys. Rev. B **65**, 092101 (2002)
[38]M. Schubert, *Infrared Ellipsometry on Semiconductor Layer Structures: Phonons, Plasmons, and Polaritons* (Springer, New York, 2004).
[39]M. J. Brett and R. R. Parsons, J. Vac. Sci. Technol. A **4**, 423 (1986).
[40]W. S. Baer, Phys. Rev. **154**, 785 (1967).
[41]S. S. Devlin, *Physics and Chemistry of II-VI Compounds*, edited by M. Aven and J. S. Prener (North Holland, Amsterdam, 1967), pp. 549.
[42]Z. Gergintschew, H. Förster, J. Kositza, and D. Schipanski, Sens. Actuators, B **26**, 170 (1995).
[43]L. Liao, H. B. Lu, J. C. Li, H. He, D. F. Wang, D. J. Fu, C. Liu, and W. F. Zhang, J. Phys. Chem. C **111**, 1900 (2007).